

Application of satellite observations for identifying regions of dominant sources of nitrogen oxides over the Indian Subcontinent

Sachin D. Ghude,¹ Santosh H. Kulkarni,¹ Chinmay Jena,¹ Gabriele G. Pfister,² G. Beig,¹ S. Fadnavis,¹ and R. J. van der A³

Received 21 March 2012; revised 28 October 2012; accepted 2 November 2012.

[1] We used SCIAMACHY (10:00 LT) and OMI (13:30 LT) tropospheric NO₂ columns to study diurnal and seasonal patterns in NO₂ concentrations over India. Using characteristics of seasonal variability in tropospheric NO₂ columns, we present a simple methodology to identify the dominant NO_x source category for specific regions in India. Regions where the dominant source category is classified as biomass burning are found generally to agree with the ATSR fire count distribution. Relating OMI NO₂ columns to surface NO_x emission, we find that biomass burning emission account for an average flux of 1.55×10^{11} molecules cm⁻² s⁻¹ during the peak burning period. Furthermore, extrapolating this estimated flux to the total burned area for the year 2005, biomass burning is estimated to account for 72 Gg of N emissions. Additional analysis of fire events in Northeast India shows a marked increase in TES retrieved O₃ concentrations, suggesting significant photochemical ozone formation during the peak biomass burning period. Regions where the dominant source type was categorized as anthropogenic are in good agreement with the distribution of major industrial regions and urban centers in India. Tropospheric NO₂ columns over these anthropogenic source regions increased by 3.8% per year between 2003 and 2011, which is consistent with the growth in oil and coal consumption in India. The OMI-derived surface NO₂ mixing ratios are indirectly validated with the surface in situ measurements (correlation $r = 0.85$, $n = 88$) obtained from the air quality monitoring network in Delhi during August 2010 to January 2011. Most of the OMI-derived surface NO₂ values agree with surface-based measurements, supporting the direct utility of OMI observation for emission estimates. Finally, we use OMI NO₂ columns to estimate NO_x emissions for selected large cities and major thermal power plants in India and compare these estimates with the INTEX-B and EDGAR emission inventory. We find that, for a few locations, OMI-derived emission show fair agreement; however, for many locations, NO_x emissions differ from INTEX-B and EDGAR inventories.

Citation: Ghude, S. D., S. H. Kulkarni, C. Jena, G. G. Pfister, G. Beig, S. Fadnavis, and R. J. van der A (2013), Application of satellite observations for identifying regions of dominant sources of nitrogen oxides over the Indian Subcontinent, *J. Geophys. Res. Atmos.*, 118, doi:10.1029/2012JD017811.

1. Introduction

[2] Nitrogen oxides (NO_x), which are formed mostly by combustion processes (e.g., power plants, vehicles, fires) and to a lesser extent by natural sources (e.g., soils, lightning), play a key role in tropospheric chemistry. They lead to ozone formation, can act as aerosol precursor, contribute

to acid rain, and affect the abundance of hydroxyl radicals (OH). Nitrogen dioxide (NO₂) also plays a role as a pollutant itself. Some epidemiological studies have shown consistent association of long-term NO₂ exposure with increased risk of respiratory symptoms [Panella *et al.*, 2000; Smith *et al.*, 2000; Gauderman *et al.*, 2002] and mortality [Burnett *et al.*, 2004; Samoli *et al.*, 2006]. NO₂ concentrations are also highly correlated with other pollutants either emitted by the same sources or formed through chemical reactions in the troposphere [Brook *et al.*, 2007]. Therefore, accurate knowledge of the global and regional distribution of various NO_x sources is required to understand better its impact on air quality and climate change.

[3] Tropospheric NO₂ observation from space began in 1995 with GOME (global ozone monitoring experiment)-1 [Burrows *et al.*, 1999] and has continued with SCIAMACHY (scanning imaging absorption spectrometer for atmospheric

¹Indian Institute of Tropical Meteorology, Pune, India.

²Atmospheric Chemistry Division, National Center for Atmospheric Research, Boulder, Colorado, USA.

³Royal Netherlands Meteorological Institute, De Bilt, Netherlands.

Corresponding author: S. D. Ghude, Indian Institute of Tropical Meteorology, Pune 411 008, Maharashtra, India. (sachinghude@tropmet.res.in)

cartography), OMI (ozone monitoring instrument) and GOME-2 measurements. These measurements have been used successfully to examine spatial and temporal patterns of NO_x emissions [Richter *et al.*, 2005; van der A *et al.*, 2006; Ghude *et al.*, 2008, 2009], to examine specific emission sources [Jaegle *et al.*, 2004, 2005; Boersma *et al.*, 2005; Martin *et al.*, 2007; van der A *et al.*, 2008; Ghude *et al.*, 2010], to provide top-down estimates of NO_x emission via inverse modeling [Martin *et al.*, 2003, 2006; Müller and Stavrou, 2005; Zhang *et al.*, 2007; Ashley *et al.*, 2010; Lamsal *et al.*, 2011], to infer NO_x lifetime [Leue *et al.*, 2001; Kunhikrishnan and Lawrence, 2004; Beirle *et al.*, 2011] or NO_x production from lightning [Boersma *et al.*, 2005; van der A *et al.*, 2008], and to estimate surface NO₂ concentrations [Lamsal *et al.*, 2008; Boersma *et al.*, 2009; Lamsal *et al.*, 2011; Lee *et al.*, 2011]. Observations of a weekly pattern in GOME tropospheric NO₂ [Beirle *et al.*, 2003] and diurnal variation in NO₂ (driven by emissions and photochemistry) from SCIAMACHY and OMI observations demonstrated the capability of detecting temporal patterns of pollution from space. Recent works have compared the SCIAMACHY, GOME [Martin *et al.*, 2006; Bucsele *et al.*, 2008], and OMI [Kramer *et al.*, 2008; Wenig *et al.*, 2008; Celarier *et al.*, 2008; Boersma *et al.*, 2009; Lamsal *et al.*, 2010; Ghude *et al.*, 2011] tropospheric NO₂ columns with coincident airborne/surface-based measurements. Each of these studies clearly suggests that the satellite-observed tropospheric NO₂ column retrievals are closely related to ground-level NO₂ concentrations and motivate its use in assessing regional distributions of dominant NO_x sources and their growth rates.

[4] For developed nations, there is rather good knowledge of NO_x sources available from existing ground-based monitoring networks. In contrast to the United States, Europe, and China, stations in the current monitoring network in India are very sparse. Large regions of India lack accurate and long-term NO₂ measurements, which poses a limit on understanding the regional patterns of dominant NO_x sources (e.g., NO_x emission from biomass burning, soil, and industries and vehicles). These observations are also insufficient for understanding better the influence of increased human activities on the NO_x growth rate over the Indian region. Satellite observations of tropospheric NO₂ are useful to address some of these issues because of their good spatial coverage and long-term measurements over the entire Indian domain.

[5] In our earlier work, we examined spatial patterns of emission hot spots, regional and global trends, and rain-induced NO_x emission from soils [Ghude *et al.*, 2008, 2009, 2011]. Expanding on our earlier work, the objective of this study is to develop a simple approach to use OMI tropospheric NO₂ column retrievals to partition dominant NO_x source regions and gain insight into the spatial pattern of partitioned NO_x sources. We build on the work of van der A *et al.* [2008] and demonstrate how satellite-derived information on the seasonal cycle of NO₂ can be used to identify the magnitude and geographic distribution of NO_x sources from biomass burning soils and fossil fuel combustion.

[6] Section 3 compares SCIAMACHY and OMI retrievals over the Indian region and try to interpret diurnal difference in terms of diurnal variation of NO_x. Section 4 discusses the

spatial distribution of dominant NO_x source types (biomass, soil, and anthropogenic) inferred from OMI measurements and quantifies the total NO_x emissions from biomass burning sources in India. In combination with retrievals of surface ozone from the Tropospheric Emissions Spectrometer (TES), we also examine the photochemical processes governing ozone formation from large biomass burning sources in Northeast India. We subsequently examine the spatial distribution of anthropogenic NO_x sources and quantify the growth rate in tropospheric NO₂ by using satellite measurements. We further compare surface measurements inferred from OMI observation with simultaneous in situ surface NO₂ measurements and show that OMI measurements can be used to estimate ground-level concentration. Finally, we use a top-down approach to infer NO_x emission for large cities and high-capacity thermal power plants in India and compare these with bottom-up estimates.

2. Satellite Observations

[7] This study uses both tropospheric NO₂ column retrieved from SCIAMACHY aboard Envisat and OMI aboard the Earth Observing System (EOS) Aura. SCIAMACHY tropospheric NO₂ is derived from nadir spectra, with a typical spatial resolution of 30 km × 60 km. It crosses the equator at 10:00 local time (LT) in descending mode and covers the globe in 6 days. We use SCIAMACHY NO₂ retrievals for 2003 – 2011 available from the Tropospheric Emission Monitoring Internet Service (TEMIS; <http://www.temis.nl>, version 2.0). In brief, slant column densities are determined with differential optical absorption spectroscopy (DOAS) in the 426.3–451.3 nm spectral window. The stratospheric (background) slant column is estimated from data assimilation of slant columns in the global chemistry-transport model TM4 [Dentener *et al.*, 2003]. After subtraction of the stratospheric slant column, the residual tropospheric slant column is translated into a tropospheric vertical column by a tropospheric air mass factor. The retrieval algorithm has been described in detail by Boersma *et al.* (2004) and Blond *et al.* (2007). Detailed error estimates and kernel information has been given by Eskes and Boersma [2003].

[8] OMI observes the atmosphere in nadir view with a local equator crossing time between 13:40 and 13:50 LT. In standard operation mode, the OMI pixel size is about 13 km × 24 km. Together with the SCIAMACHY 10:00 LT, this provides valuable information on the diurnal cycle in NO₂. The OMI dense spatial coverage and higher spatial resolution increase the likelihood of encountering cloud-free scenes [Krijger *et al.*, 2007]. Two independent tropospheric NO₂ column data products from OMI observations are currently available. These data products are available from the NASA-GES-DAAC (OMI standard product) and from TEMIS (DOMINO product). We use the DOMINO (Dutch OMI NO₂) product (v2.0) available at <http://www.temis.nl> [Boersma *et al.*, 2011] for the years 2005 – 2011. Slant columns are determined with the DOAS algorithm in the absorption spectrum of a window of 365 – 500-nm solar radiation [Boersma *et al.*, 2007]. The contribution of stratospheric NO₂ is then removed [Bucsele *et al.*, 2006; Boersma *et al.*, 2007]. The air mass factor (AMF) corrects for viewing geometry and light-scattering interferences such as clouds and aerosol particles. This AMF is applied

to convert the measured slant columns into tropospheric vertical column densities. OMI retrieval errors have an absolute component of $\sim 1.0 \times 10^{15}$ molecules cm^{-2} and a relative (AMF) component of 30% [Boersma *et al.*, 2007]. Further details on retrievals and error budget have been discussed by Boersma *et al.* [2007].

[9] In addition to OMI and SCIAMACHY data, we include tropospheric ozone retrievals from the TES. TES was launched into sun-synchronous orbit aboard Aura on 15 July 2004. TES provides a global view of tropospheric trace gas profiles [Worden *et al.*, 2004], with measurements available since 2005. An overview of the TES retrieval algorithm and error estimation has been provided by Bowman *et al.* [2006]. Tropospheric ozone retrievals from TES have been validated against ozonesonde and lidar measurements, and it was found that the values are positively biased upward by as much as 15% from the surface to the upper troposphere (1000 to 100 hpa) compared with ozonesonde data [Worden *et al.*, 2009; Boxe *et al.*, 2010]. Nassar *et al.* [2008] have shown that TES O₃ is biased upward by 9.6 ppb in the lower troposphere. The current study used the TES level 3 (L3) version 1.0 data product at the surface level (available at <http://gdata1.sci.gsfc.nasa.gov/>). Further details on retrievals and algorithms for producing TES level 3 data have been provided by Luo *et al.* [2007].

3. Intercomparison

3.1. Comparison of SCIAMACHY and OMI NO₂ Retrievals Over the Indian Region

[10] Here we compare the spatial distribution of OMI and SCIAMACHY tropospheric NO₂ (version 2.0) over the Indian region. Both data sets use a common algorithm for tropospheric NO₂ retrievals. Further details on the retrievals have been provided by Boersma *et al.* [2011]. For the monthly average data (for OMI and SCIAMACHY), only pixels with a cloud radiance fraction of less than 50% (cloud fraction less than ~ 0.2) and solar zenith angle (SZA) of less than 80° are used. Data affected by the row anomalies and

data pixels with a snow surface are not included. Our interest here is to examine diurnal variation in NO₂ observed from these satellite instruments. The main differences between the OMI and the SCIAMACHY observations are indeed the local overpass time and the resolution. The wavelengths used (for OMI 405–465 nm and SCIAMACHY 426.3–451.3 nm) for the retrieval are same, and there is no significant difference between OMI and SCIAMACHY retrievals from fitting the modeled spectrum to the measured reflectance differences of these instruments [Boersma *et al.*, 2008]. The overpass time affects the ratio between the OMI (13:30 LT) and SCIAMACHY (10:00 LT) observation [Boersma *et al.*, 2008, 2009] and provides information on diurnal variation of NO_x emissions and chemistry, depending on the source of NO₂ (anthropogenic, soil, or biomass burning). The spatial resolution of OMI is variable, between $24 \times 13 \text{ km}^2$ and $24 \times 120 \text{ km}^2$, depending on the position within the swath. The SCIAMACHY resolution is $30 \times 60 \text{ km}^2$. Therefore, it is important to be aware of these differences. The sensitivity of OMI and SCIAMACHY instruments are quite comparable, and the averaging kernels of OMI and SCIAMACHY are very much alike. Cloud parameters for OMI and SCIAMACHY are retrieved with somewhat different algorithms, which shows a small difference in cloud-top pressure (OMI on average higher by 60 hPa) [Boersma *et al.*, 2007]; however, the differences between NO₂ retrievals are expected to be very small for the scenes with a cloud radiance fraction of less than 50% [Boersma *et al.*, 2008].

[11] Figure 1a and 1b shows the mean tropospheric NO₂ column amounts from SCIAMACHY ($0.25^\circ \times 0.25^\circ$) and OMI ($0.125^\circ \times 0.125^\circ$) over the Indian region, averaged over the 2005–2010 period. SCIAMACHY and OMI mean tropospheric NO₂ columns have similarities in their spatial distribution, with pronounced enhancements ($> 4.5 \times 10^{15}$ molecules cm^{-2}) over major industrial regions, over metropolitan areas, and over large coal-based thermal power plants. Both observe large-scale pollution over the densely populated northern plain (Indo-Gangetic

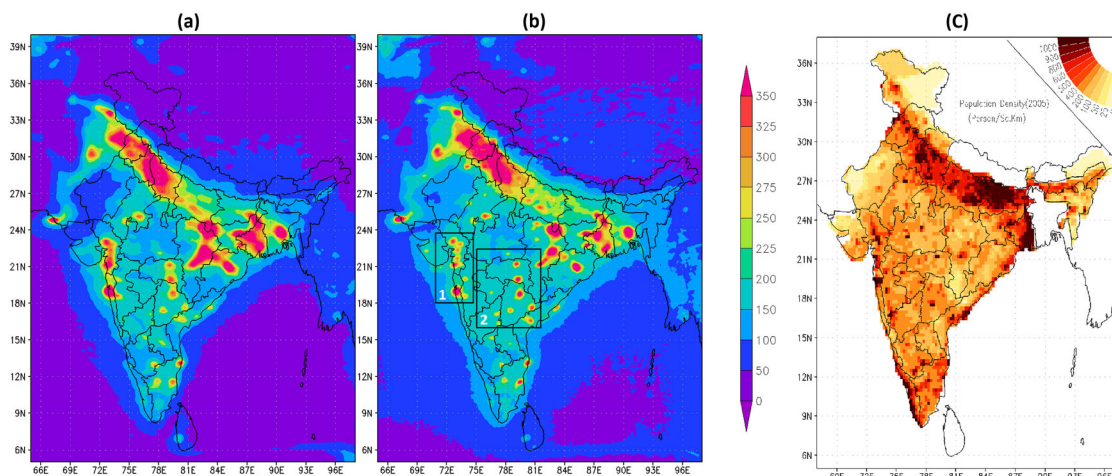


Figure 1. Tropospheric NO₂ (1×10^{13} molecules cm^{-2}) annual climatology (2005 – 2010) over India as observed from (a) SCIAMACHY at $0.25^\circ \times 0.25^\circ$ and (b) OMI at $0.125^\circ \times 0.125^\circ$ grid resolution. Box-1 indicates the Mumbai-Gujarat industrial corridor region and box-2 a central and southern Indian region with a high localization of cities and industrial centers. (c) Population density (persons/ km^2) of India, 2005 (data source: <http://sedac.ciesin.columbia.edu/gpw>).

[IG] region) of India (see Figure 1c) and lower values ($<1.5 \times 10^{15}$ molecules cm^{-2}) over the central Madhya Pradesh, western Rajasthan, and northeastern India (Assam, Arunachal Pradesh, Manipur, etc.), where population density is low. Both exhibit a similar seasonal cycle (not shown) with a minimum during monsoon season (JJAS) reflecting the shorter lifetime and wet removal of NO_x [Crutzen and Lawrence, 2000]. A detailed analysis of emission hot spots in India and their seasonal variation has been provided by Ghude *et al.* [2008]. Compared with SCIAMACHY, OMI tropospheric NO₂ columns reveal a clearer picture because of the higher resolution. For example, OMI NO₂ resolves pollution from individual cities along the Mumbai-Gujarat Industrial corridor (marked as region 1) and many localized point sources (cities or medium-capacity thermal power plants) from central and southern India (marked as region 2).

[12] Figure 2 shows scatterplot of OMI and SCIAMACHY both mapped on the same grid scale ($0.25^\circ \times 0.25^\circ$) over the Indian region. The inset shows the frequency distribution of the absolute differences between SCIAMACHY and OMI overlaid by a Gaussian fit line. The spatial distributions of OMI and SCIAMACHY mean tropospheric NO₂ columns are highly correlated, with a correlation coefficient of $r^2=0.93$. We find that $\sim 79\%$ (Gaussian fit centered at -0.21) of the OMI values within this region are higher than SCIAMACHY values, with differences generally in the range between 0 to -0.4×10^{15} molecules cm^{-2} .

3.2. Diurnal Variation

[13] Figure 3a shows the absolute difference between SCIAMACHY and OMI mean tropospheric NO₂ columns for the 2005–2010 period averaged over a $0.25^\circ \times 0.25^\circ$ grid. Figure 3b is the same as Figure 3a, but the absolute difference is plotted for winter months only (December–January average). Wintertime SCIAMACHY NO₂ column amounts are generally higher than OMI over large fossil fuel source regions, which is particularly pronounced over urban/suburban areas in India such as Delhi, Hyderabad, Bangalore, Mumbai, Ahmedabad, Pune, etc. On an annual

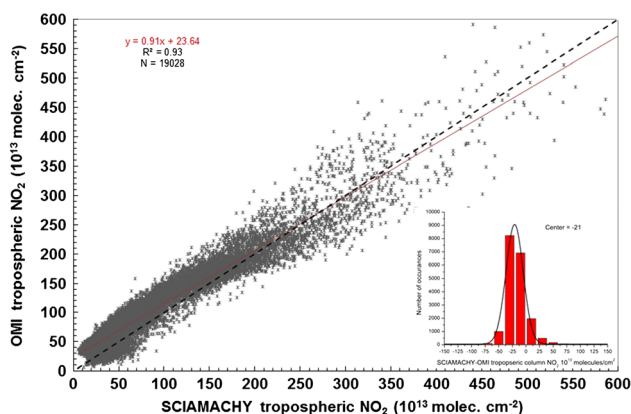


Figure 2. Scatterplot of SCIAMACHY tropospheric NO₂ vs. OMI tropospheric NO₂ averaged for 2005–2010. Each point represents the monthly mean value for a $0.25^\circ \times 0.25^\circ$ grid cell over the region 5–28°N and 67–98°E. The inset shows a histogram plot of the absolute differences between SCIAMACHY and OMI (vertical bars bin size = 0.2).

scale, OMI and SCIAMACHY show smaller differences. SCIAMACHY NO₂ columns are also higher than OMI over the marine region downwind of Mumbai, reflecting a strong diurnal cycle in NO₂ in the marine boundary layer.

[14] These differences might be attributed to the diurnal variation of tropospheric NO₂. Over large cities in India, NO_x concentrations peak during daytime and reach a minimum in late afternoon, reflecting the diurnal cycle in rush-hour traffic emission and photochemical loss processes [Reddy *et al.*, 2009; Purkait *et al.*, 2009; Sharma *et al.*, 2010]. The OMI overpass time is 3 h later than SCIAMACHY, and by the time of the OMI overpass more NO₂ has been removed from the atmosphere than at the time of the SCIAMACHY overpass. These results also appear consistent with findings of Boersma *et al.* [2008] over fossil fuel source regions at northern midlatitude, where SCIAMACHY observed 5–40% higher NO₂ than OMI. Furthermore, Boersma *et al.* [2008] showed that higher SCIAMACHY NO₂ columns than OMI over fossil fuel cannot be attributed to retrieval artifacts. Difference between mean tropospheric NO₂ columns measured by SCIAMACHY and OMI (Figure 3a) are less over relatively less populated and less polluted areas (see Figure 1c).

[15] In some cases, OMI shows higher NO₂ columns over coal-fired power plants, particular those power plants (individual or clustered in a small area) with power generation capacity greater than 1800 MW (circles in Figure 3b). These power plants appear as hot spots also in the annual average. A similar diurnal difference (not shown here) is also seen in the model simulation [Ghude *et al.*, 2012; manuscript in preparation]. Boersma *et al.* [2008] studied thermal power plants in the southern United States and attributed the higher OMI NO₂ columns to a maximum in NO_x emission in the afternoon. However, in India, thermal power plants do not exhibit such a diurnal cycle, and it would be expected that OMI columns are smaller than those of SCIAMACHY because of increased chemical loss at midday. The reasons for OMI retrieving higher NO₂ columns than SCIAMACHY over these power plants are not clear and should be investigated further. Downwind of these high-capacity thermal power plants (winds are northeasterlies during winter), however, SCIAMACHY NO₂ columns are higher than OMI NO₂ columns, reflecting a strong diurnal cycle. Over the remote Indian Ocean, where there is minimum variability, we find that SCIAMACHY tropospheric NO₂ columns are on average 0.22×10^{15} molecules cm^{-2} lower than OMI columns.

4. Source Attribution

[16] Each source of NO_x has specific characteristics that determine its seasonal variability, and this information can be used to identify the dominant source type of NO_x emissions [van der A *et al.*, 2008]. This section analyzes the seasonal cycle in OMI tropospheric NO₂ columns over regions where the dominant source type is known. The sources considered here are biomass burning, anthropogenic sources, and soil. Figure 4 shows three example of the seasonal cycle (climatology 2005–2010) in tropospheric NO₂ columns for selected locations dominated by biomass burning (Figure 4a), soil (Figure 4b), and anthropogenic (Figure 4c) sources. In India, the seasonal cycle of NO_x over the regions

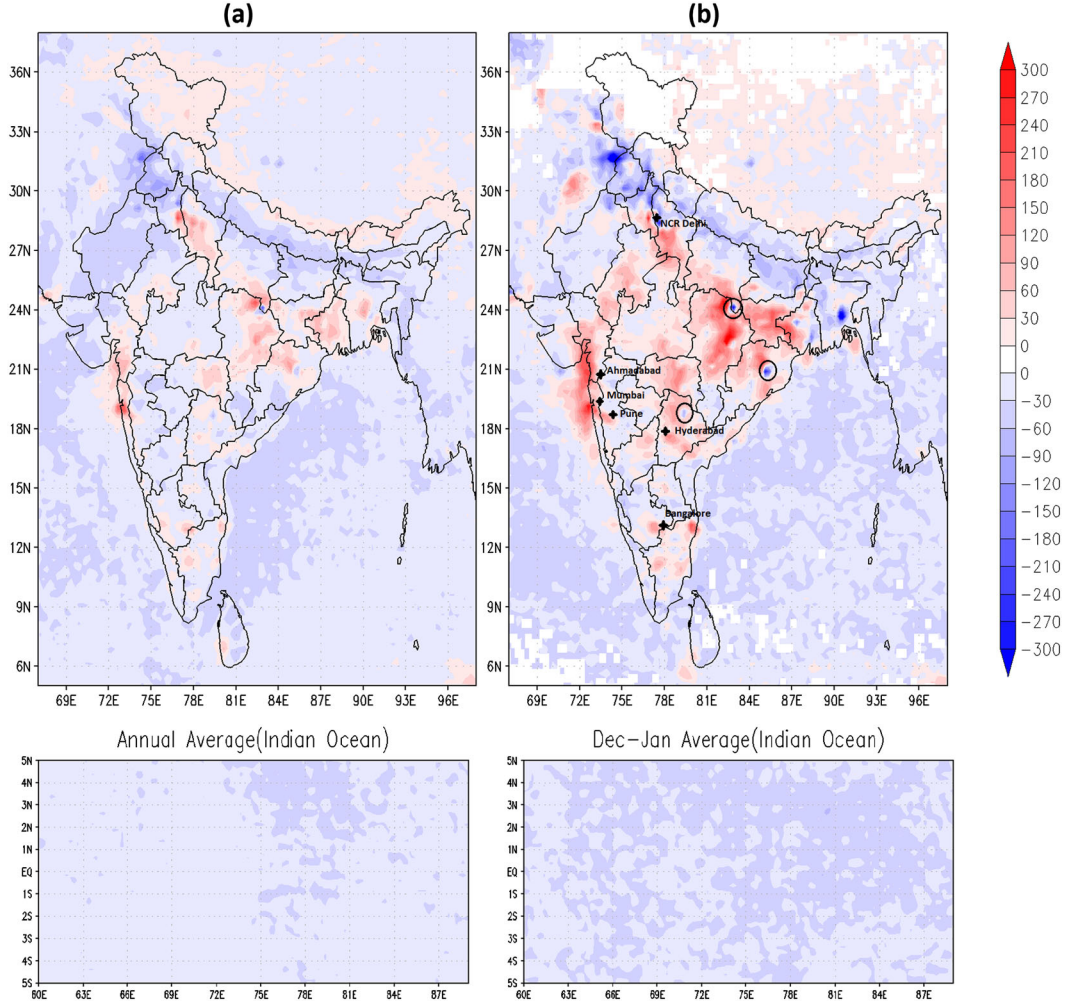


Figure 3. Absolute difference between SCIAMACHY and OMI tropospheric NO₂ column over India. (a) Annual mean difference for 2005 – 2010 and (b) mean difference for winter months only (December–January 2005 – 2010). Both SCIAMACHY and OMI data are averaged over a $0.25^\circ \times 0.25^\circ$ grid. Circles indicate high-capacity thermal power plants, and stars correspond to cities. Bottom panels show the difference between SCIAMACHY and OMI tropospheric NO₂ over the Indian Ocean (5°S – 5°N , 60 – 90°E) annually and for winter seasons.

dominated by biomass burning, soil, and anthropogenic typically has its maximum in March – April [Venkataraman *et al.*, 2006; Ghude *et al.*, 2010], June (onset of summer monsoon) [Ghude *et al.*, 2010], and December – January [Ghude *et al.*, 2008], respectively. This is reflected in Figure 4, showing that each NO_x source type has its own signature in the annual cycle. Figure 4a shows the signals of NO_x emission from biomass burning for a region in the northeastern (92 – 96°E , 21 – 27°N) and central (76 – 78°E , 20 – 22°N) parts of India. Similarly, Figure 4b shows the signals of NO_x emission for a region in central Madhya Pradesh (75 – 80°E , 22 – 24°N), and Figure 4c shows signals of NO_x emission from anthropogenic emission for the industrialized cities Mumbai, Delhi, and National Capital Region (NCR; 75 – 80°E , 27 – 30°N).

[17] With examination of the seasonal cycle, we use a simple set of classification rules to identify the dominant source type of NO_x. A grid is identified as dominated by biomass burning, anthropogenic, or soil sources if the month of maximum NO₂ coincides with March – April,

December – January, or June, respectively. The general expression for the decision criteria can be written as:

$$[\text{OMI}_{\text{NO}_2\text{max}}]_1^{12} - \text{OMI}_{\text{NO}_2}(m) = 0, \quad (1)$$

where $m=1, 2, 3 \dots 12$; where $[\text{OMI}_{\text{NO}_2\text{max}}]_1^{12}$ is the maximum tropospheric NO₂ amount at every grid cell observed between January (month number 1) and December (month number 12) for the study year; and where $\text{OMI}_{\text{NO}_2}(m)$ is the tropospheric NO₂ for the month m in that year (for example, $\text{OMI}_{\text{NO}_2}(1)$ represents tropospheric NO₂ amount for the month of January). Applying this equation to each OMI grid cell will return a zero value according to the dominant source in a particular grid and thus provides the information on the dominant source category for that grid.

4.1. Biomass Burning

[18] Biomass burning both from forested areas and from croplands in India occurs mainly during February – May. Cropland burning varies with geographic location,

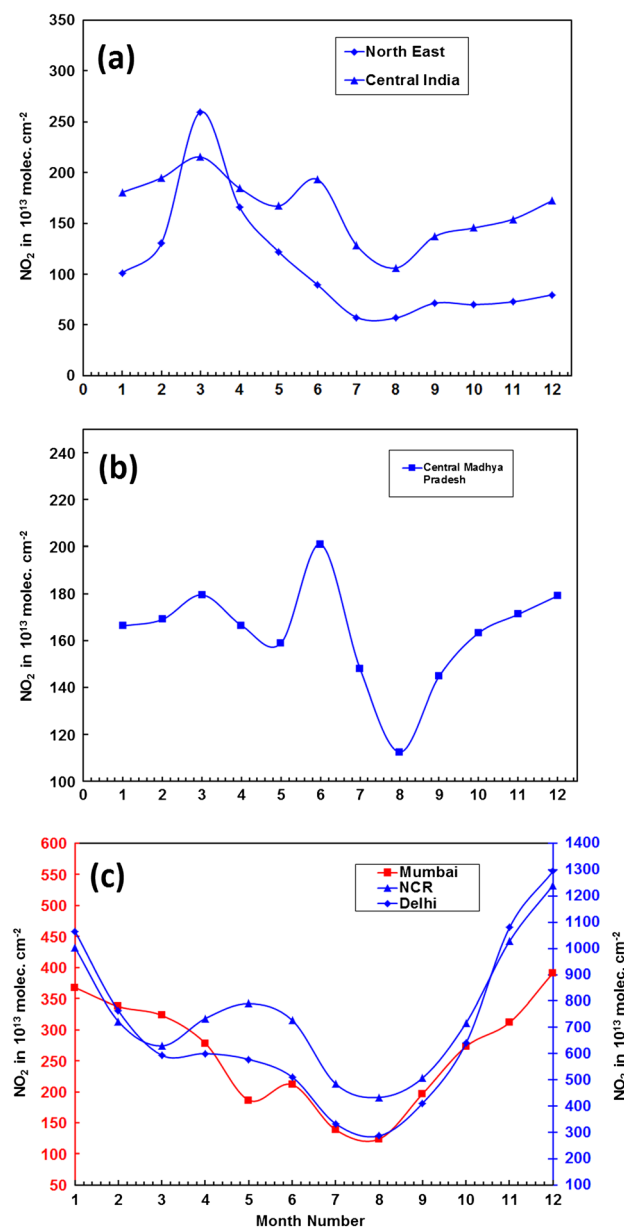


Figure 4. Mean seasonal variation (2005 – 2010) of OMI tropospheric NO₂ column averaged over selected regions dominated by (a) biomass burning, (b) soil, and (c) anthropogenic NO_x emission.

corresponding to major harvesting seasons in the region, but is predominant in March and April [Venkataraman *et al.*, 2006; Ghude *et al.*, 2010]. Figure 5a shows areas with a March – April maximum during 2005 and represents a spatial distribution that likely can be attributed to NO_x emissions from biomass burning, with lesser contributions from other sources. Tropospheric NO₂ columns over these grid cells (representative of biomass burning) are in the range of about $2 - 3 \times 10^{15}$ molecules cm⁻². Most of these grid cells are found to represent regions where either population density is low or large industrial activities are not present. Regions characterized as biomass burning are found generally to agree with the distribution of Along Track Scanning Radiometer (ATSR) fire counts ($0.5^\circ \times 0.5^\circ$; Figure 5b). The distribution observed in Figure 5a and 5b

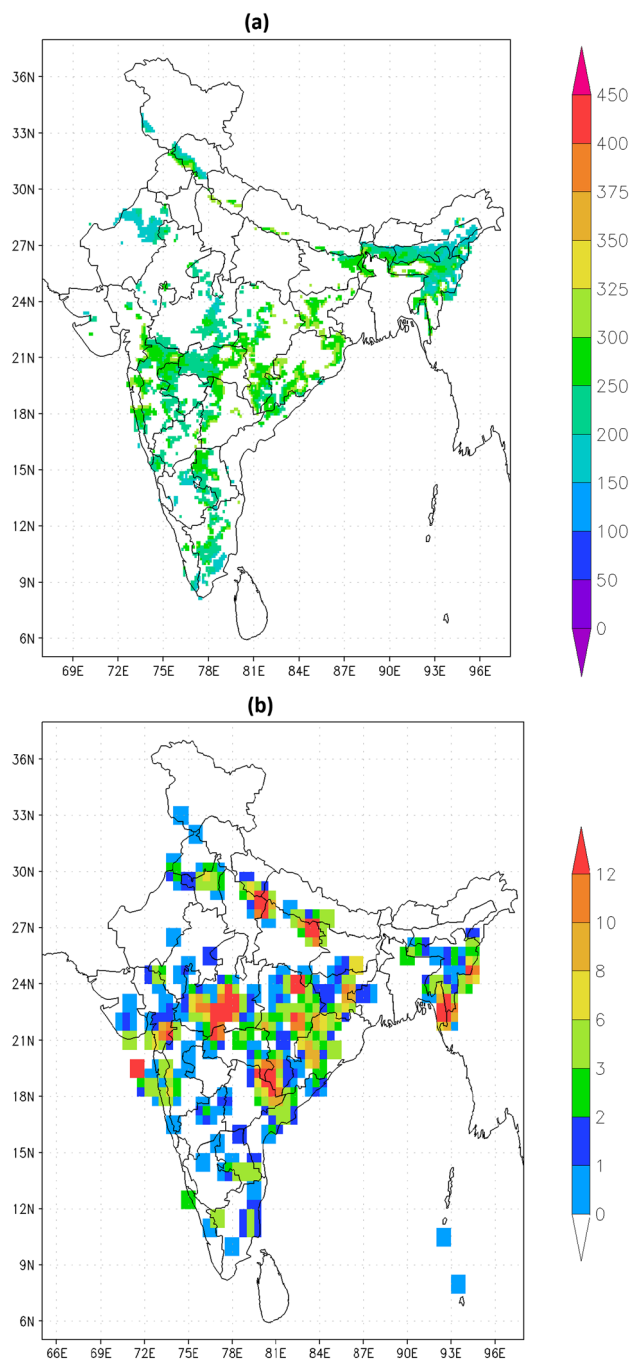


Figure 5. (a) Spatial distribution of OMI NO₂ (1×10^{13} molecules cm⁻²) for 2005 for regions with a maximum in the seasonal cycle in tropospheric NO₂ during March April. For these regions the dominant source type is estimated as biomass burning. (b) ATSR fire counts over the India region during March – April 2005 over a $0.5^\circ \times 0.5^\circ$ grid.

reflects what is known about forest and cropland burning patterns in India [Venkataraman *et al.*, 2006]. It can be seen from Figure 5a that most of the Northeast region ($92 - 96^\circ\text{E}$, $21 - 27^\circ\text{N}$) shows biomass burning as a dominant source of NO_x emission. Average tropospheric NO₂ columns in this region reach up to $\sim 2.6 \times 10^{15}$ molecules cm⁻². ATSR fire data also show high fire frequency in this region. NO_x from biomass burning in central India,

southern India, and eastern India is also captured well in the OMI observations. It can be seen in Figure 5a that the identification scheme fails over parts of the central and western Indo-Gangetic plain. In this region, the dominating source of NO_x is emissions from strong anthropogenic activity. The longer lifetime of NO₂ in winter compared with summer results in a pronounced seasonal maximum in December ($\sim 5.8 \times 10^{15}$ molecules cm⁻²) and a less pronounced peak ($\sim 4 - 4.3 \times 10^{15}$ molecules cm⁻²) for the biomass burning period. This region will be discussed in more detail in section 4.3.

4.1.1. Estimation of NO_x emissions from biomass burning

[19] To estimate the NO_x emission from biomass burning, we focus on the northeastern part of India (92 – 96°E, 21 – 27°N). NO_x sources in this rural area are not as sharply localized as in most other regions, and the region is characterized by low population density and minor industrial/vehicular activities. On annual average, tropospheric NO₂ columns are low over this region and close to the detection limit of the satellite retrievals ($\sim 1.2 \times 10^{15}$ molecules cm⁻²; Figure 1). Almost 90% of the area in this region is occupied by dense forest (Joshi, 1991), and large forest fires generally occur during the dry seasons. As discussed above, fire frequency peaks in March, with OMI average tropospheric NO₂ columns reaching up to 2.6×10^{15} molecules cm⁻², well above the detection limit of the satellite retrievals. For a more detailed investigation of biomass burning-induced NO_x enhancement, we examined the day-to-day variation of OMI tropospheric NO₂ columns averaged over the study area. Figure 6 shows the time series of OMI tropospheric NO₂ columns for cloud fractions less than 0.2 during 2005 (data with cloud radiance fraction <50% and SZA <80° are used, and data affected by the row anomalies and data pixels with a snow surface are not included). A clear seasonal enhancement in tropospheric NO₂ columns is evident during biomass burning season (mid-February to mid-April), in agreement with previous studies [Venkataraman, et al., 2006; Chand Kiran et al., 2006], followed by lower column amounts in the remaining seasons. The graph shows a large day-to-day variability during

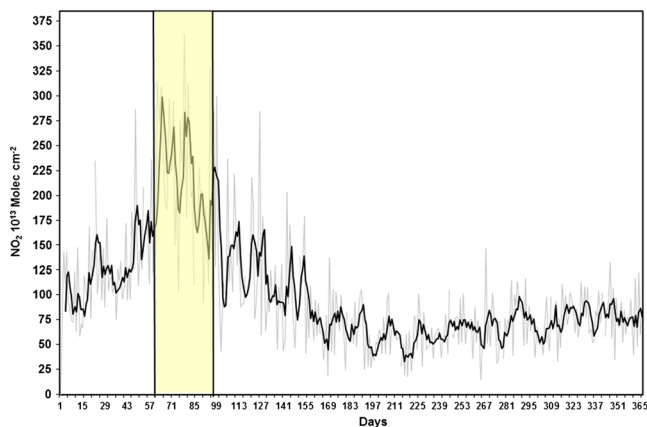


Figure 6. Day-to-day variation of OMI tropospheric NO₂ VCDs averaged over a northeastern region of India for the year 2005. The gray line denotes daily values and the black line a 5-day running mean.

burning season, reflecting the variable nature of fires. Tropospheric NO₂ columns as high as 3.6×10^{15} molecules cm⁻² (18 March) have been observed by OMI during the peak fire season. Mean biomass burning-induced NO_x enhancement during the peak burning period is about 3×10^{15} molecules cm⁻².

[20] During March, air masses traveling into this region are generally from the west; i.e., the selected region is downwind of strong anthropogenic sources (e.g., the city Dhaka). However, surface wind shows stagnant patterns over this region, with low wind speeds (mean wind speed 1.5 m/s; <http://facstaff.unca.edu/>), and we expect the transport of anthropogenic emissions to have a small effect. We evaluated the contribution of transported anthropogenic pollution from the nearby point source (Dhaka) using the relationship

$$T_{\text{NO}_2} = \text{OMI}_{\text{NO}_2} \times \exp(-t/\tau_{\text{NO}_x}), \quad (2)$$

where OMI_{NO_2} is the tropospheric NO₂ column over the nearby anthropogenic region, t is the transport time between a nearby region and the study region (calculated using mean wind speed [~ 1.5 m/s]), and τ_{NO_x} is the NO_x lifetime (~ 7 h over tropics in March [Martin et al., 2003]). The horizontal distance between Dhaka and the study region is >250 km, yielding a contribution of transported NO_x less than 5%. We therefore assume that NO_x emissions in this region during March are exclusively associated with biomass burning. Our estimate is to be considered as an upper limit, because some local nonburning sources are present; however, the interference from these sources is expected to be small.

[21] To estimate the NO_x emissions from biomass burning, we relate the OMI tropospheric NO₂ columns to surface NO_x emission using an inverse method as described by Martin et al. [2003]. This method has been used successfully to estimate NO_x emissions from various sources such as anthropogenic sources, soils, etc., in recent years (Martin, 2003; Müller and Stavrou, 2005; Jaegle et al., 2004, 2005; Zhang et al., 2007; Ashley et al., 2010; Ghude et al., 2010; Lamsal et al., 2011; Lee et al., 2011). Top-down NO_x emission, E , can be inferred by mass balance through a linear relationship between E and retrieved tropospheric NO₂ column OMI_{NO_2} :

$$E = \alpha \text{OMI}_{\text{NO}_2}, \quad (3)$$

where,

$$\alpha = (T_{\text{NO}_x}/T_{\text{NO}_2})/\tau_{\text{NO}_x} \quad (4)$$

T_{NO_x} and T_{NO_2} in equation (4) are the tropospheric NO_x and NO₂ columns, respectively; and τ_{NO_x} is the NO_x lifetime. We obtained the $T_{\text{NO}_x}/T_{\text{NO}_2}$ ratio here from the MOZART-4 model simulation (simulation results are taken from <http://www.acd.ucar.edu/wrf-chem/mozart.shtml>), close to satellite overpass time for March for the study region. The MOZART-4 simulations used here are from the standard simulation described by Emmons et al. [2010]. The model is driven by NCEP/NCAR-reanalysis meteorology and uses emissions based on POET, REAS, and GFED2 [see Emmons et al., 2010]. These results are available at $2.8^\circ \times 2.8^\circ$ horizontal resolution and give output for every 6 h. We assumed NO_x lifetime of 7 h [Martin et al., 2003] to calculate α from equation (4). Horizontal transport of NO_x from the surrounding areas over the study region, which smears the local relationship between NO₂ column and

NO_x emission, is a source of error in the application of equation 3. As discussed above, the effect of the horizontal transport is likely to be smaller than the estimated biomass burning emission signal. Therefore, we neglect the effect from horizontal transport of NO_x.

[22] Using equation 3, the resulting NO_x emissions from biomass burning is estimated to account for an average flux of 1.55×10^{11} molecules $\text{cm}^{-2} \text{s}^{-1}$ during the peak burning period. By further relating the average flux of 1.55×10^{11} molecules $\text{cm}^{-2} \text{s}^{-1}$ to the area burned product from MODIS (MCD45A1) [Roy *et al.*, 2002] for all of India, we can estimate the amount of NO_x emissions from open biomass burning in India. The annual estimate of MCD45A1 burned area (forest, shrubland, grassland, and cropland) for India during 2005 is approximately 62,200 km^2 [Chang and Song, 2010]. This leads to an estimated emission of 72 Gg (N) yr^{-1} from biomass burning in India for the year 2005. The total NO_x emissions from biomass burning in India are estimated to be 114 Gg (N) yr^{-1} and 91 Gg (N) yr^{-1} in the EDGAR (v4.2) and GICC emission inventories (for 2005), respectively, which is somewhat higher than the estimate made in the present study using top-down approach. On the other hand, emission from biomass burning in India is estimated to be 32 Gg (N) yr^{-1} in the GFEDV3.1 and 260 Gg (N) yr^{-1} in the NCAR fire emission inventory (FINN) [Wiedinmyer *et al.*, 2011], which differ significantly from the estimate made in the present study. The difference between our estimate and EDGAR/GFEDV3.1 may be due to the fact that the uncertainty associated with the emission estimate from NO₂ satellite data results from uncertainties regarding the size of the burned area, fuel load, combustion factor, and type of vegetation burned. Furthermore, the uncertainty in the retrieval of the tropospheric NO₂, uncertainty in the lifetime of NO₂, and uncertainty in NO_x/NO₂ column ratio derived from the model are expected to add additional uncertainty to the top-down estimate. OMI retrieval uncertainties are stated to be about 30 – 60%, whereas it is difficult to assess the uncertainty of the satellite-derived burned area product [Hoelzemann *et al.*, 2004]. Table 1 shows an example of an annual estimate of NO_x emission from biomass burning in India derived from the GFEDv3.1 [Giglio *et al.*, 2010] burned area product during the period 2005 – 2010. It can be seen that there is significant year-to-year variability in NO_x emission from biomass burning in India.

4.1.2. Photochemical ozone formation in biomass burning season

[23] Biomass burning is believed to be an important source of ozone precursors such as CO and NO_x [Crutzen and

Carmichael, 1993]. Here, we examine the photochemical production of ozone resulting from extensive biomass burning using daily averaged O₃ retrievals at the surface level from TES (L3, v2.0) and tropospheric NO₂ measured by OMI, together with ATSR fire counts [Arino *et al.*, 2011] for the period January 2006 to December 2007. As described above, our analysis focuses on the Northeast region in India, and satellite data provide essential information to gain more insight into the area's sources and chemical characteristics.

[24] Figure 7 (top) shows day-to-day variations of surface ozone and tropospheric NO₂ averaged over the study region for 2006 – 2007 (5-day running mean), and Figure 7 (bottom) shows ATSR fire counts for the same period. Lowest ozone values (~30 – 40 ppbv) are found during monsoon season from about June to August. The Indian summer monsoon leads to influx of relatively clean air masses of marine origin, and heavy precipitation and less solar radiation lead to washout of precursor gasses and less photochemical ozone

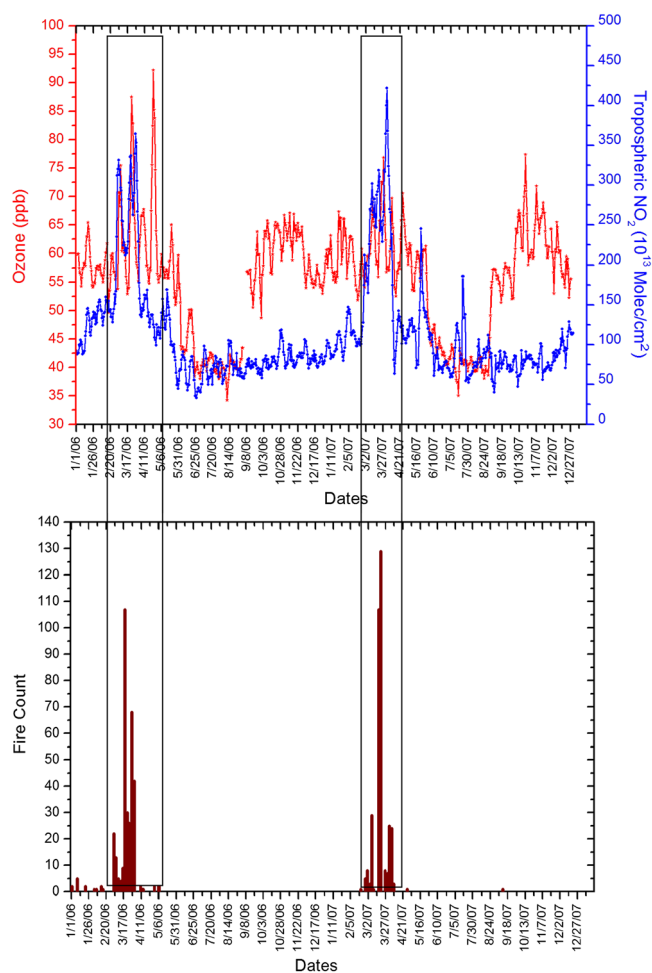


Table 1. NO_x Emission Estimate From Biomass Burning Derived From the GFEDv3.1 Burnt Area Product

Year	Burnt Area (Sq.Km) (GEFDv3.1)	Emission Estimate Gg (N) yr^{-1}
2005	28,141	32.3
2006	22,318	25.6
2007	34,309	39.4
2008	34,462	39.5
2009	36,518	41.9
2010	50,202	57.6

Figure 7. Time series of daily OMI (blue) tropospheric NO₂ VCDs and TES (red) retrieved ozone (surface level retrieval) averaged over a region in Northeast India (92 – 96°E, 21 – 27°N) for January 2006 to December 2007 (top) and ATSR fire count totals over the same region (bottom).

formation. In about September, ozone levels again start increasing, reaching $\sim 55 - 65$ ppbv during September–February. These higher ozone levels can be attributed mostly to the prevailing wind pattern during the postmonsoon and winter season, which transports ozone from the northeastern part of the IG region as well as from East Asia to the study region.

[25] During the biomass burning season around March, significantly enhanced levels of ozone, up to $75 - 90$ ppbv, are seen. The enhancement in ozone is consistent with a significant increase, up to $3.4 - 4.5 \times 10^{15}$ molecules cm^{-2} , in tropospheric NO₂ columns during the same period. Given the timing, it can be inferred that both enhancements in surface ozone and NO₂ columns are associated with biomass burning, indicating that precursors emitted from biomass burning together with the abundance of sunlight lead to significant photochemical ozone production.

[26] To identify changes in ozone that are associated with changes in tropospheric NO_x from fire emissions, we have selected only those observations for which at least one fire is detected in the study area based on ATSR fire counts. In Figure 8, we show correlations between TES surface ozone and OMI tropospheric NO₂ for these criteria. A positive correlation ($R=0.68$, $n=36$) is seen between O₃ and NO₂, indicating that variations in O₃ mixing ratios during the fire events are influenced primarily by NO_x emissions from biomass burning sources in this region. The slope of the linear fit between ozone and NO_x suggests an increase of ~ 6 ppbv of ozone per 1×10^{15} molecules cm^{-2} in tropospheric NO₂. It should be noted that, although TES can detect ozone both in the lower and in the upper troposphere, TES retrievals are less sensitive to lower tropospheric ozone [Worden *et al.*, 2004], with a positive bias up to 10 ppb or more [Nassar *et al.*, 2008; Boxe *et al.*, 2010]. Because of this, confidence in the surface level data is limited. Increase in surface ozone during the fire events, however, demonstrates that, even with the limited sensitivity to surface ozone retrievals, TES is able to detect photochemical ozone formation during fire events.

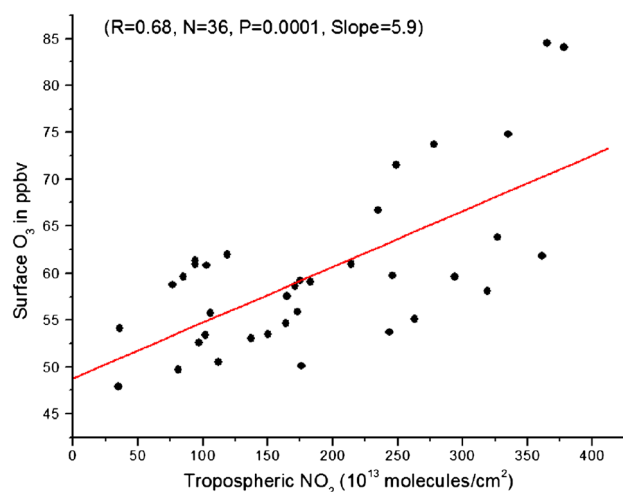


Figure 8. Relationship between tropospheric NO₂ and ozone for fire events between 2005 and 2008 averaged over a northeastern ($92 - 96^\circ\text{E}$, $21 - 27^\circ\text{N}$) region of India. The regression analysis parameters are given in the figure.

4.2. Soil Emission

[27] Soil emission of NO_x can be expected to be an important source in regions with agriculture and grassland [Yienger and Levy, 1995; van der A *et al.*, 2008]. Yienger and Levy [2005] showed that the soil NO_x emissions are temperature and moisture dependent and are augmented by the use of fertilizer [Bertram *et al.*, 2005] and by pulsing as a sudden increase in NO_x measured after rainfall [Jaegle *et al.*, 2004]. In a recent study in India, Ghude *et al.* [2010] showed that bursts in soil NO_x emission occur after the onset of summer monsoon rainfall and have a maximum in the months of May and June. The spatial distributions of regions where soil emissions are estimated to be the dominant source type are shown in Figure 9. We include this result here for completeness but do not provide a detailed analysis; this has been provided by Ghude *et al.* [2010].

4.3. Anthropogenic Emission

[28] Seasonal cycles in NO_x over fossil fuel source regions have their maximum typically in December–February because of the longer lifetime of NO_x in the tropics during winter season [Martin *et al.*, 2003; van der A *et al.*, 2008]. A clear seasonal maximum in the month of December or January is seen over strong anthropogenic source regions such as Delhi, Mumbai, and the NCR (Figure 4c). A similar winter maximum in NO_x has also been reported with ground-based in situ measurement from urban locations in India [e.g., Ghude *et al.*, 2008; Purkait *et al.*, 2009; Sharma *et al.*, 2010; David and Nair, 2011]. The

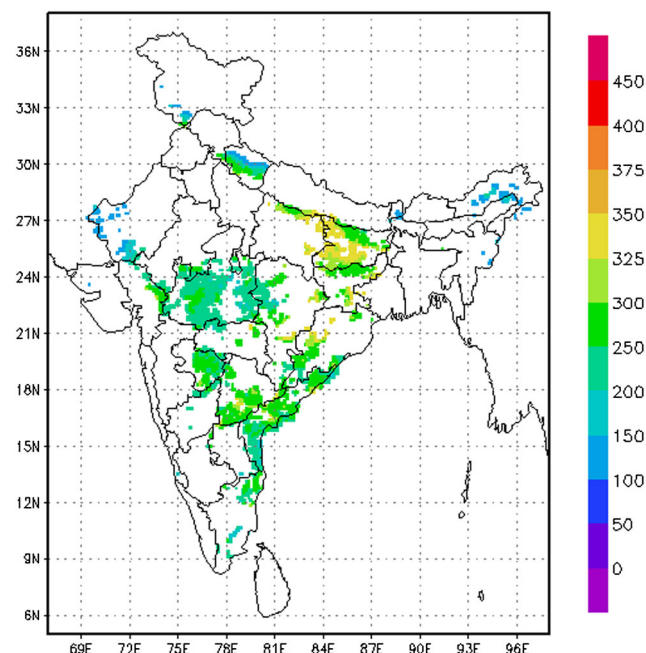


Figure 9. Spatial distribution of OMI NO₂ (1×10^{13} molecules cm^{-2}) for 2005 for regions with a maximum in the seasonal cycle in tropospheric NO₂ during June. For these regions, the dominant source type is estimated as soil emissions.

seasonality for the NCR region in Figure 4c shows a secondary maximum in MAM. This secondary maximum corresponds to contributions from NO_x emissions from biomass burning, although the dominant source of NO_x is still from fossil fuel combustion. The seasonal minimum in the month of July–August over these locations can be attributed to wet removal of NO_x during summer monsoon [Crutzen and Lawrence, 2000; Paramee *et al.*, 2005].

[29] When we apply equation (1) to each grid cell, it yields a spatial distribution of NO₂ observations that can likely be attributed to NO_x emission from anthropogenic sources without contributions from other sources (Figure 10). NO₂ columns over these grid cells are on the order of 3.5×10^{15} molecules cm⁻² or higher. The defined regions represent most of the major industrial regions and urban centers and agree well with independent major emission hot spots shown in Figure 11. Figure 10 distinguishes anthropogenic emission from the Mumbai-Gujarat industrial corridor, from western and eastern parts of the IG region, and from individual hot spots that are representative of large-capacity thermal power plants and large cities in India. Close examination of Figures 10 and 11 reveals that anthropogenic emissions from the western part of the IG region are dominated largely by vehicular sources (transportation sector), whereas anthropogenic emissions from the eastern part of the IG region seem to be dominated mostly by emissions from thermal power plants [Ghude *et al.*, 2008]. Anthropogenic emissions from the Mumbai-Gujarat industrial corridor include contributions from both the power/industrial sector and the transportation sector.

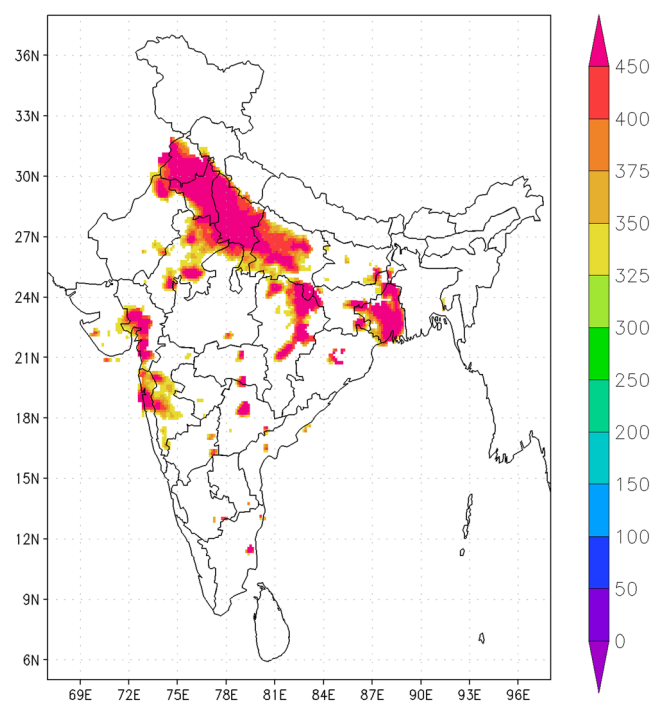


Figure 10. Spatial distribution of OMI (1×10^{13} molecules cm⁻²) for 2005 for regions with a maximum in the seasonal cycle in tropospheric NO₂ during December–January. For these regions, the dominant source type is estimated as anthropogenic.

4.3.1. Trend in anthropogenic NO₂ emissions

[30] To estimate trends in anthropogenic NO_x, we use OMI observations over India for the period 2005–2011. Since SCIAMACHY covers a longer time period than OMI, we have also estimated the trend between 2003 and 2011 by using the SCIAMACHY observation. We further select only those grids cells in Figure 1b that are representative of urban centers and industrial locations. Over most of the urban centers and major industrial locations, mean tropospheric NO₂ columns are above 3.5×10^{15} molecules cm⁻², as can be seen from Figure 10. Therefore, we defined all grids in which tropospheric NO₂ columns are above 3.5×10^{15} molecules cm⁻² as representative of high anthropogenic activity. The ratio of total NO₂ column over the selected region to the total NO₂ column over India is observed to be 0.58. Monthly mean tropospheric NO₂ columns over these grids are averaged to obtain a single time series for the Indian region. A linear model [Ghude *et al.*, 2011] with a seasonal component is used to fit the time series. The time series of NO₂ is represented by the function

$$\theta(t) = \alpha(t) + \beta(t) \cdot \text{trend}(t) + \text{resid}(t).$$

[31] Here, $\theta(t)$ represents the monthly mean NO₂ column of month t , and $\alpha(t)$ time-dependent 12-month seasonal coefficients and $\beta(t)$ are the time-dependent 12-month trend coefficients for the NO₂ time-series [trend(t)]. Resid(t) represents the residual or noise. Figure 12 shows an example of the monthly and annual averaged time series (OMI [red] and SCIAMACHY [blue]) for the Indian region. There is a clearly increasing trend in anthropogenic NO_x emission over India. OMI and SCIAMACHY show a growth rate of $2.9\% \pm 1.9\% \text{ yr}^{-1}$ and $3.8\% \pm 2.2\% \text{ yr}^{-1}$ and are found to be significant at the two-sigma error level. This estimate is comparable to the growth rate in NO_x emission estimated in bottom-up inventories such as EDGAR (v4.2; $4.2\% \text{ yr}^{-1}$), GAINS ($3.6\% \text{ yr}^{-1}$), or Garg *et al.* [2006] ($4.4\% \text{ yr}^{-1}$) and can be attributed to the growth in power, transportation, and industrial sectors in India. According to the U.S. Energy Information Administration (EIA; available at <http://www.eia.gov/cfapps/ipdbproject>) estimate, oil consumption in India has increased from ~ 2.3 million barrels/day in 2003 to ~ 3.2 million barrels/day in 2010 (approximately a 39% increase). Similarly, coal consumption increased by about 65% between 2003 and 2010.

4.3.2. Comparison with ground-based measurements

[32] Our interest here is to compare the OMI tropospheric NO₂ measurements with coincident surface-based in situ NO₂ measurements from urban regions and to quantify further the NO_x emissions from specific point sources (such as large cities and high-capacity thermal power plants). We use hourly averaged ambient concentrations of NO₂ measured at four different sites in Delhi as part of the Ministry of Earth Sciences System of Air Quality Forecasting and Research (SAFAR; <http://safar.tropmet.res.in/>), Government of India's air quality monitoring project for the Commonwealth Games (CWG) in 2010 (3–14 October). This is the only data set available to us for comparison and poses a limitation in our comparison. At these sites, ambient NO₂ was monitored from 23 September 2010 to 10 January 2011 using standard chemiluminescence NO_x analyzer

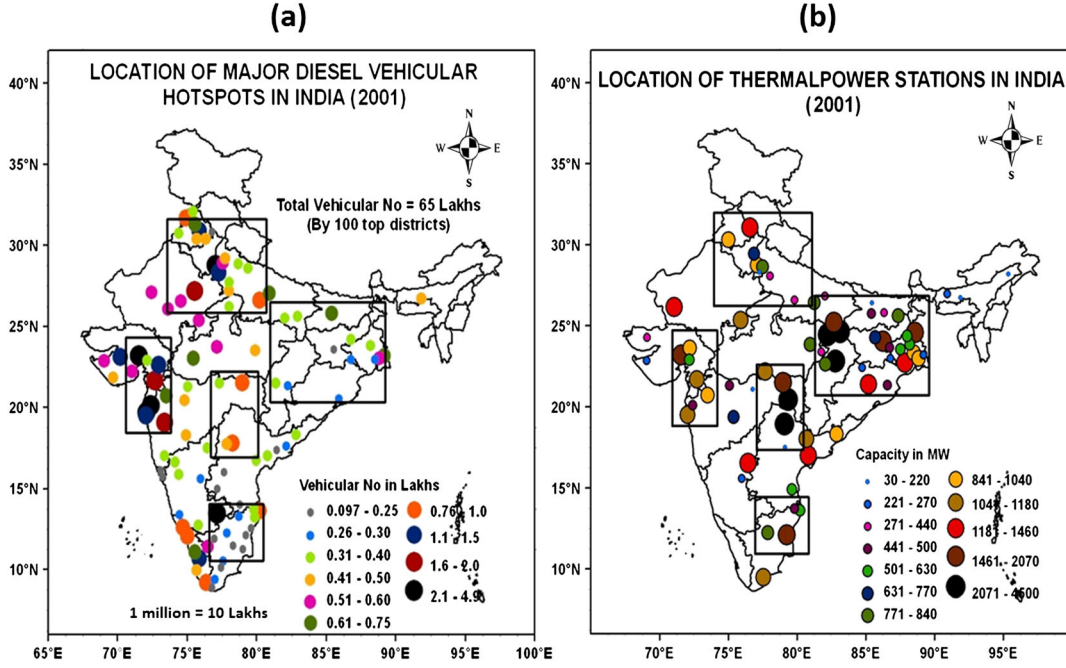


Figure 11. Locations of major hot spots in India where emissions are dominated by (a) vehicular sources or (b) thermal power plants. (Source: *Sahu* [2010].)

using molybdenum converters. NO₂ is catalytically converted to NO on a heated molybdenum surface and then measured as NO by chemiluminescence after reaction with ozone. Calibration of the instrument was performed every other day using external calibration cylinders with a multi-point calibration technique during the measurement period. For the comparison, the nearest OMI pixels to each measurement site are selected and averaged for a given day. Furthermore, we averaged the NO₂ in situ measurements over 12:00 – 14:00 LT (from all four sites) to correspond to the OMI overpass. We exclude comparisons for pixels with cloud radiance fractions greater than 0.2 as well as for the days when surface-based measurements were not taken. In total 88 measurements remain following the filtering processes. The molybdenum converter also partially converts the other oxidized nitrogen compounds (such as HNO₃, PAN) to NO_x and can overestimate NO₂, particularly in the afternoon [*Dumlea et al.*, 2007]. We do not have the means to correct the surface concentrations but interpret them as an upper limit for the true NO₂ concentrations. Direct comparison of NO₂ columns retrieved from OMI with surface NO₂ measurements taken in Delhi are highly correlated, with a correlation coefficient of 85% (not shown here).

[33] For a more quantitative comparison for ground-based data with tropospheric vertical column densities (VCDs) from OMI, OMI measurements were scaled to NO₂ mixing ratios measured at the surface using the procedure described by *Lamsal et al.* [2008]. *Lamsal et al.* [2008] inferred surface-level NO₂ concentration (S) from OMI tropospheric vertical column densities (Ω) by applying the ratio of surface-level NO₂ concentration (S_G) to vertical column density (Ω_G) calculated by a global model as:

$$S = (S_G/\Omega_G) \times \Omega. \quad (5)$$

[34] Here we infer surface NO₂ from OMI measurements with WRF-Chem simulations over Delhi [*Beig et al.*, in preparation] using above relationship. WRF-Chem simulations were conducted as part of the MoES SAFAR project. Again we find a high correlation and agreement when surface measurements are compared with surface NO₂ derived from OMI NO₂ columns using equation (5) ($r=0.85$, $n=88$, $p=0.0001$, slope=0.87; see Figure 13a and 13b).

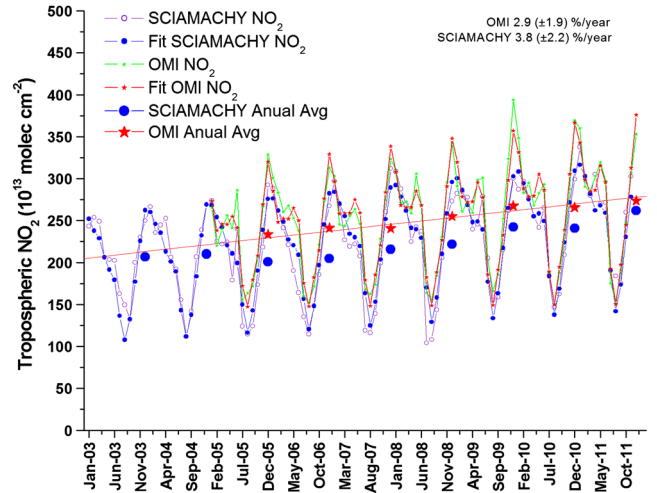


Figure 12. SCIAMACHY (measured [purple] and fitted [blue]) and OMI (measured [green] and fitted [red]) time series of tropospheric NO₂ averaged over major anthropogenic source regions in India for 2003 – 2011 and 2005 – 2011, respectively. Annual mean SCIAMACHY (blue) and OMI (red) tropospheric NO₂ columns are shown for the same period.

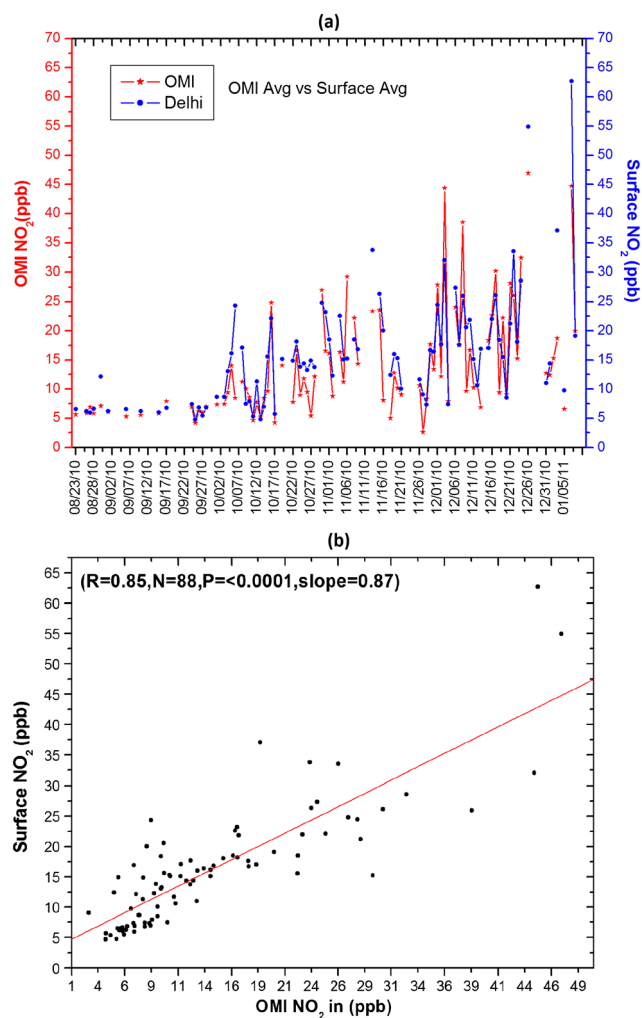


Figure 13. (a) Comparison of OMI inferred surface NO₂ (red) with surface in situ NO₂ measurements (blue) averaged from four monitoring sites in Delhi (from 23 September 2010 to 10 January 2011). (b) Correlation between OMI inferred surface NO₂ and surface NO₂.

Outliers in Figure 13a and 13b likely reflect transport and free tropospheric processes. Table 2 summarizes the average difference between surface NO₂ calculated from OMI NO₂ with respect to surface-based NO₂ measurements, as well as minimum and maximum difference during the study period. The mean and maximum differences between surface-NO₂ and OMI-derived NO₂ are approximately 2 ppb and 30 ppb, respectively. Most of the OMI-derived surface NO₂ values (85%) agree with surface-based measurements to within 30%. The slope in Figure 13b (0.87) indicates that surface NO₂ measurements are lower than OMI-derived surface NO₂ over the study region. Given the fact that surface NO₂ measurements with molybdenum converter overestimates NO₂ concentration, our OMI-derived NO₂ values are higher than the surface measurements. This may be caused by the uncertainties introduced by the ratio of surface-level NO₂ concentration to vertical column density calculated by the model in equation (5). Given these statistics, the agreement between OMI observations and surface measurements is significant and supports the feasibility of using surface measurements in validating day-to-day variations in satellite-derived NO₂.

Table 2. Comparison Between Surface NO₂ Concentrations Inferred From OMI Tropospheric NO₂ VCDs and Surface In Situ NO₂ Measurements

	Average	SD (±)	Min	Max
OMI Trop NO ₂ (10 ¹⁵ molecules/cm ²)	8.30	8.3	1.6	27.9
OMI _{Sur} NO ₂ (ppb)	13.9	9.3	2.6	46.9
Surface NO ₂ (ppb)	16	9.9	4.7	62.6
OMI_{Sur} – Surface NO₂ (ppb)	–2.1	5.7	–18.3	27.9

4.3.3. Estimation of NO_x emissions from specific point sources

[35] In the next step, we estimate NO_x emission for a set of large cities and high-capacity thermal power plants using OMI observations. We consider only power plants that are located in rural regions and away from large urban centers. We adopt a mass balance approach [Leue *et al.*, 2001; Martin *et al.*, 2003] and consider cloud-free (cloud fraction 20%) NO₂ tropospheric column retrievals averaged for December 2006. To infer the NO_x emission by mass balance requires information on the tropospheric NO_x to NO₂ ratio and the lifetime of NO_x as stated in equation (4). Here we assume a typical NO/NO₂ ratio of 0.32 [Seinfeld and Pandis, 2006] and a lifetime of approximately 5 h [Spicer, 1982; Beirle *et al.*, 2011] under urban conditions at noon. We also attempted to estimate this ratio using the WRF-Chem model and found NO/NO₂ ratio of 3.16 over strong anthropogenic source regions. Recently, Sharma *et al.* [2011] reported a similar NO/NO₂ ratio (0.31) based on surface measurements in Delhi, confirming that our choice of the NO/NO₂ ratio considered in this study is reasonable. It should be noted here that uncertainty in the retrieval of the tropospheric NO₂, site-specific NO/NO₂ ratio, and lifetime of NO₂ is a source of error in application of equation (4) and is expected to add uncertainty to the top-down estimate. However, this method provides first-hand information about the NO_x emission from the large point sources and can be used for verifying emission estimates from other bottom-up inventories. Table 3 presents the derived NO_x emission *E* for individual large cities and thermal power plants and comparison with two bottom-up emission inventories: the Intercontinental Chemical Transport Experiment-Phase B (INTEX-B) and EDGAR(V4.2). INTEX-B provides emission on a 0.5° × 0.5° grid, and the EDGAR data set consists of 0.1° × 0.1° gridded emissions. For comparing the emissions, we regridded the OMI observations and EDGAR emissions on 0.5° × 0.5° resolution. Among the cities considered, the highest emission has been estimated for Delhi (14.2 × 10¹¹ molecules cm^{–2} s^{–1}), which is in fair agreement with INTEX-B (11.8 × 10¹¹ molecules cm^{–2} s^{–1}) [Zhang *et al.*, 2009]. Total emissions from the EDGAR inventory for Delhi are 21.4 × 10¹¹ molecules cm^{–2} s^{–1}, much higher than INTEX-B and our estimate. For Kolkata, the top-down estimate is a factor of 1.5 and 2.6 lower than the INTEX-B and EDGAR emissions, respectively. Among the thermal power plant sources considered, the derived emissions for Talcher, Korba, and Kota are in generally good agreement with the INTEX-B estimates. EDGAR emissions are, however, a factor 4 higher than the top-down estimate over these locations (except for Kota, which is lower than our estimate by a factor of 3). EDGAR emissions from Satpura, Raichur, and Nagpur are in good agreement with the top-down

Table 3. NO_x Emission Estimate for Individual Point Sources (Cities and Thermal Power Plants [TPP] on 0.5×0.5 Grid Resolution) From the Top-Down Approach (This Study), INTEX-B, and EDGAR(v4.2) Inventories for 2006

Location	Top-Down(10^{11} Molecules $\text{cm}^{-2} \text{s}^{-1}$)	INTEX-B(10^{11} Molecules $\text{cm}^{-2} \text{s}^{-1}$)	EDGARv4.2(10^{11} Molecules $\text{cm}^{-2} \text{s}^{-1}$)
<i>Cities</i>			
Delhi	14.3	11.8	21.4
Mumbai	6.3	1.0	8.1
Kolkata	5.4	8.1	14.3
Banglore	3.8	2.1	5.1
Hyderabad	2.7	0.9	1.7
Punducherry	3.8	1.6	15.8
Chennai	3.4	4.7	8.0
Kanpur	3.1	0.8	2.2
<i>TPP</i>			
Singrauli + Rihnd + Orba	7.6	4.7	21
Talcher	5.6	5.6	22.9
Korba	5.6	6.3	19.7
Ramaguddam	4.0	2.8	15.8
Chandrapur	3.2	—	15.0
Kota	3.5	4.1	1.1
Nagpur	3.2	1.1	5.5
Raichur	3	7.8	7.0
Satpura	2.6	0.3	6.6

estimate, but INTEX-B shows a large difference. Several cities (e.g., Mumbai, Hyderabad, Kanpur, Pondicherry) and power plant sources (e.g., Ramagundam, Chandrapur, collective emission from Singrauli, Rihand, and Orba, etc.) show large deviations between top-down and INTEX-B and/or EDGAR emissions. For example, our top-down estimate for Mumbai city is about 6.3×10^{11} molecules $\text{cm}^{-2} \text{s}^{-1}$, which is of the order of magnitude expected according to anthropogenic activity in the city [Sahu, 2010] and is comparable to EDGAR emissions. However, INTEX-B emissions are lower by a factor of 6.

5. Conclusions

[36] In this study, for the first time, we compare the SCIAMACHY and OMI tropospheric NO₂ column retrievals over India and present a spatial assessment of different NO_x sources. Both instruments observe similar spatial patterns of NO₂ hot spots, but OMI reveals more clear structures because of its higher spatial resolution. We also find that wintertime SCIAMACHY NO₂ column amounts are generally higher than OMI over large urban/suburban areas and over the marine boundary layer downwind of strong emission sources, reflecting diurnal variation in chemistry and emissions.

[37] We show that characteristics of seasonal variability in NO₂ can be exploited to examine dominant NO_x source types on a regional scale. We have developed a simple classification scheme to identify regions dominated by biomass burning, soil, and anthropogenic NO_x emission sources. Regions characterized as biomass burning are found to generally agree with the distribution of ATSR fire counts over India. Relating OMI NO₂ columns in Northeast India to surface NO_x emissions using an inverse method, we found that biomass burning emission account for an average flux of 1.55×10^{11} molecules $\text{cm}^{-2} \text{s}^{-1}$ during the peak burning period. Extrapolating this flux to the total MODIS (MCD45A1) estimate of burned area for India for the year 2005 (62,200 km²), we estimate 72 Gg of N Yr⁻¹ emissions from the biomass burning. This is on the order of but lower

than the EDGAR estimate of 112 Gg (N) and the GICC estimate of 90 Gg (N) for the same year. A significant enhancement in ozone concentrations during biomass burning season in Northeast India was found, suggesting photochemical ozone formation from fire-emitted precursors with an increase of ~ 6 ppb of ozone per 1×10^{15} molecules cm^{-2} increase in tropospheric NO₂. Similarly, using the classification scheme, we inferred regions dominated by anthropogenic NO_x sources and found these generally to agree the locations of major industrial regions and urban centers in India. We find a growth rate of $3.8\% \pm 2.2\% \text{ yr}^{-1}$ between 2003 and 2011 for anthropogenic sources, which is related to the growth in oil and coal consumption in India. This growth rate is comparable with the estimate made by EDGAR (V4.2; $4.2\% \text{ yr}^{-1}$), GAINS ($3.6\% \text{ yr}^{-1}$), or Garg *et al.* [2006] ($4.4\% \text{ yr}^{-1}$) emission inventories. We further show that surface in situ measurements from monitoring networks in urban locations can provide useful information to validate indirectly NO₂ column measurements from space and could be used to estimate NO_x emission for hot spot regions. We estimated NO_x emission for a set of large cities and high-capacity thermal power plants, relating OMI observations to surface NO_x emission. The comparison of top-down estimated emission with the INTEX-B inventory for a few locations such as Delhi, Bangalore, Chennai Korba, Talcher, and Kota shows overall fair agreement but differs significantly for areas such as Mumbai, Hyderabad, Kanpur, Ramagundam, and Chandrapur. Similarly, comparison between top-down estimated emission with the EDGAR inventory shows fair agreement for locations such as Mumbai, Kanpur, and Bangalore but significantly differ for the other locations.

[38] This work illustrates the promise of our approach for understanding the spatiotemporal variability of NO_x sources in India and for indirect validation of satellite products. Additional ground-based in situ NO₂ observations over a wide geographical area would be useful to increase our understanding of the spatiotemporal variability of emissions, transport, and photochemistry over the Indian region and to support analysis and validation of satellite retrievals. This

study provides further incentive to re-examine NO_x emissions from hot spot sources in India to identify and constrain uncertainties in current emission inventory.

[39] **Acknowledgments.** We thank Prof. B. N. Goswami, Director, IITM, for his encouragement during the course of the study. The ATSR-WFA fire count data used in this study were acquired from the Data User Element of the European Space Agency. We acknowledge EC-JRC/PBL EDGAR (v4.2; <http://edgar.jrc.ec.europa.eu/>) was used for country-level emission estimates. We also acknowledge Global Fire Emissions Database version 3 (GFED3) and GICC for providing fire emissions through GEIA/ACCENT data portal activity. The authors thank the atmospheric science data center, NASA, for providing TES data. One of the authors (S.D.G.) thanks the Department of Science and Technology (DST) for a BOY-SCAST fellowship to conduct this work.

References

- Arino O., S. Casadio, and D. Serpe (2011), Global night-time fire season timing and fire count trends using the ATSR instrument series, *Remote Sensing Environ.*, doi:10.1016/j.rse.2011.05.025.
- Ashley R. R., V. C. Lukas, E. J. Bucsela, M. O. Wenig, and R. C. Cohen (2010), Space-based constraints on spatial and temporal patterns of NO_x emissions in California, 2005–2008 *Environ. Sci. Technol.*, *44*, 3608–3615, doi:10.1021/es903451j.
- Beirle, S., U. Platt, M. Wenig, and T. Wagner (2003), Weekly cycle of NO₂ by GOME measurements: a signature of anthropogenic sources, *Atmos. Chem. Phys.*, *3*, 2225–2232.
- Beirle, S., K. F. Boersma, U. Platt, M. G. Lawrence, and T. Wagner (2011) Megacity emissions and lifetimes of nitrogen oxides probed from space, *Science*, *333*, 1737–1739, doi:10.1126/science.1207824.
- Bertram, T. H., A. Heckel, A. Richter, J. P. Burrows, and R. C. Cohen (2005), Satellite measurements of daily variations in soil NO_x emissions, *Geophys. Res. Lett.*, *32*, L24812, doi:10.1029/2005GL024640.
- Blond, N., K. F. Boersma, H. J. Eskes, R. J. van der A, M. Van Roozendaal, I. De Smedt, G. Bergametti, and R. Vautard (2007), Intercomparison of SCIAMACHY nitrogen dioxide observations, in situ measurements and air quality modeling results over Western Europe, *J. Geophys. Res.*, *112*, D10311, doi:10.1029/2006JD007277.
- Boersma, K. F., H. J. Eskes, and E. J. Brinksma (2004), Error analysis for tropospheric NO₂ retrieval from space, *J. Geophys. Res.*, *109*, D04311, doi:10.1029/2003JD003962.
- Boersma, K. F., H. J. Eskes, E. W. Meijer, and H. M. Kelder (2005), Estimates of lightning NO_x production from GOME satellite observations, *Atmos. Chem. Phys.*, *5*, 2311–2331.
- Boersma, K. F., H. J. Eskes, J. P. Veefkind, E. J. Brinksma, R. J. van der A, M. Sneep, G. H. J. van den Oord, P. F. Levelt, P. Stammes, J. F. Gleason, and E. J. Bucsela (2007), Near-real time retrieval of tropospheric NO₂ from OMI, *Atmos. Chem. Phys.*, *7*, 2113–2128, sref:1680-7324/acp/2007-7-2103.
- Boersma, K. F., D. J. Jacob, H. J. Eskes, R. W. Pinder, J. Wang, and R. J. van der A (2008), Intercomparison of SCIAMACHY and OMI tropospheric NO₂ columns: Observing the diurnal evolution of chemistry and emissions from space, *J. Geophys. Res.*, *113*, D16S26, doi:10.1029/2007JD008816.
- Boersma, K. F., D. J. Jacob, M. Trainic, Y. Rudich, I. DeSmedt, R. Dirksen, and H. J. Eskes (2009), Validation of urban NO₂ concentrations and their diurnal and seasonal variations observed from the SCIAMACHY and OMI sensors using in situ surface measurements in Israeli cities, *Atmos. Chem. Phys.*, *9*, 3867–3879.
- Boersma, K. F., H. J. Eskes, R. J. Dirksen, R. J. van der A, J. P. Veefkind, P. Stammes, V. Huijnen, Q. L. Kleipool, M. Sneep, J. Claas, J. Leitao, A. Richter, Y. Zhou, and D. Brunner (2011), An improved retrieval of tropospheric NO₂ columns from the Ozone Monitoring Instrument, *Atmos. Meas. Techniq.*, *4*, 1905–1928.
- Boxe, C. S., J. R. Worden, K. W. Bowman, S. S. Kulawik, J. L. Neu, W. C. Ford, G. B. Osterman, R. L. Herman, A. Eldering, D. W. Tarasick, A. M. Thompson, D. C. Doughty, M. R. Hoffmann, and S. J. Oltmans (2010), Validation of northern latitude Tropospheric Emission Spectrometer stare ozone profiles with ARC-IONS sondes during ARCTAS: sensitivity, bias and error analysis, *Atmos. Chem. Phys.*, *10*, 9901–9914.
- Brook, J. R., R. T. Brunett, T. F. Dann, S. Cakmak, M. S. Goldberg, X. Fan, and A. J. Wheeler (2007), Further interpretation of the acute effect of nitrogen dioxide observed in Canadian time series studies, *J. Expos. Sci. Environ. Epidemiol.*, *17*, S36–S44.
- Bucsela, E. J., E. A. Celarier, M. O. Wenig, J. F. Gleason, J. P. Veefkind, K. F. Boersma, and E. J. Brinksma (2006), Algorithm for NO₂ vertical column retrieval from the Ozone Monitoring Instrument, *IEEE Trans. Geosci. Remote Sens.*, *44*, 1245–1258.
- Bucsela, E. J., A. E. Perring, R. C. Cohen, K. F. Boersma, E. A. Celarier, J. F. Gleason, M. O. Wenig, T. H. Bertram, P. J. Wooldridge, R. Dirksen, and J. P. Veefkind (2008), Comparison of tropospheric NO₂ in situ aircraft measurements with near-real-time and standard product data from the Ozone Monitoring Instrument, *J. Geophys. Res.*, *113*, D16S31, doi:10.1029/2007JD008838.
- Burnett, R. T., D. Steib, J. R. Brook, S. Cakmak, R. Dales, M. Raizenne, R. Vincent, and T. Dann (2004), The short-term effects of nitrogen dioxide on mortality in Canadian cities, *Arch. Environ. Health*, *59*, 228–237.
- Burrows, J. P., M. Weber, M. Buchwitz, V. Rozanov, A. Ladstatter-Weissenmayer, A. Richter, R. De Beek, R. Hoogen, K. Bramstedt, K. W. Eichmann, M. Eisinger, and D. Perner (1999), The Global Ozone Monitoring Experiment GOME: Mission concept and first scientific results, *J. Atmos. Sci.*, *56*, 151–175.
- Bowman, K. W., et al. (2006), Tropospheric emission spectrometer: Retrieval method and error analysis, *IEEE T. Geosci. Remote Sens.*, *44*, 1297–1307.
- Celarier, E. A., et al. (2008), Validation of ozone monitoring instrument nitrogen dioxide columns, *J. Geophys. Res.*, *113*, D15S15, doi:10.1029/2007JD008908.
- Chand Kiran, T. R., K. V. S. Badarinarath, V. Krishna Prasad, M. R. S. Murthy, C. D. Elvidge, and B. J. Tuttle (2006), Monitoring forest fires over the Indian region using Defense Meteorological Satellite Program Operational Linescan System nighttime satellite data, *Remote Sensing Environ.*, *103*, 165–178.
- Chang, D. and Y. Song (2010), Estimates of biomass burning emissions in tropical Asia based on satellite-derived data, *Atmos. Chem. Phys.*, *10*, 2335–2351.
- Crutzen, P. J., G. R. Carmichael (1993), Modeling the influence of fires on atmospheric chemistry, in *Fire in the Environment. The Ecological, Atmospheric and Climatic Importance of Vegetation Fires*, edited by P. J. Crutzen, J. G. Goldammer, pp. 89–106, Wiley, New York.
- Crutzen, P. J., and M. G. Lawrence (2000), The impact of precipitation scavenging on the transport of trace gases: A 3-dimensional model sensitivity study, *J. Atmos. Chem.*, *37*, 81–112, doi:10.1023/A:1006322926426.
- David, L. M., and P. R. Nair (2011), Diurnal and seasonal variability of surface ozone and NO_x at a tropical coastal site: Association with mesoscale and synoptic meteorological conditions, *J. Geophys. Res.*, *116*, D10303, doi:10.1029/2010JD015076.
- Dentener, F., W. Peters, M. Krol, M. van Weele, P. Bergamaschi, and J. Lelieveld (2003), Interannual variability and trend of CH₄ lifetime as a measure of OH changes in the 1979–2003 period, *J. Geophys. Res.*, *108*(D15), 4442, doi:10.1029/2002JD002916.
- Dunlea, E. J., et al. (2007), Evaluation of nitrogen dioxide chemiluminescence monitors in a polluted urban environment, *Atmos. Chem. Phys.*, *7*, 2691–2704.
- Emmons, L. K., S. Walters, P. G. Hess, J. F. Lamarque, G. G. Pfister, D. Fillmore, C. Granier, A. Guenther, D. Kinnison, T. Laepple, J. Orlando, X. Tie, G. Tyndall, C. Wiedinmyer, S. L. Baughcum, and S. Kloster (2010), Description and evaluation of the Model for Ozone and Related Chemical Tracers, version 4 (MOZART-4), *Geosci. Model Dev.*, *3*, 43–67.
- Eskes, H. J., and K. F. Boersma (2003), Averaging kernels for DOAS total column satellite retrievals, *Atmos. Chem. Phys.*, *3*, 1285–1291.
- Garg, A., P. R. Shukla, and M. Kapshe (2006), The sectoral trends of multigas emissions inventory of India, *Atmos. Environ.*, *40*, 4608–4620, doi:10.1016/j.atmosenv.2006.03.045
- Gauderman, W. J., et al. (2002), Association between air pollution and lung function growth in southern California children: Results from a second cohort, *Am. J. Respir. Crit. Care Med.*, *166*, 76–84.
- Ghude, S. D., S. Fadnavis, G. Beig, S. D. Polade, and R. J. van der A (2008), Detection of surface emission hot spots, trends, and seasonal cycle from satellite-retrieved NO₂ over India, *J. Geophys. Res.*, *113*, doi:10.1029/2007JD009615.
- Ghude, S. D., R. J. Van der A, G. Beig, S. Fadnavis, and S. D. Polade (2009), Satellite derived trends in NO₂ over the major global hotspot regions during the past decade and their inter-comparison, *Environ. Pollut.*, *157*, 1873–1878.
- Ghude, S. D., D. M. Lal, G. Beig, R. J. van der A, and D. Sable (2010), Rain-induced soil NO_x emission from India during the onset of the summer monsoon: A satellite perspective, *J. Geophys. Res.*, *115*, doi:10.1029/2009JD01336.
- Ghude S. D., P. S. Kulkarni, S. H. Kulkarni, S. Fadnavis, and R. J. Van Der A (2011), Temporal variation of urban NO_x concentration in India during the past decade as observed from space, *Int. J. Remote Sensing*, *32*, 849–861, doi:10.1080/01431161.2010.517797.
- Giglio, L., J. T. Randerson, G. R. van der Werf, P. S. Kasibhatla, G. J. Collatz, D. C. Morton, and R. S. DeFries (2010), Assessing variability and long-term trends in burned area by merging multiple satellite fire products, *Biogeosciences*, *7*, 1171–1186.

- Hoelzemann, J. J., M. G. Schultz, G. P. Brasseur, C. Granier, and M. Simon (2004), Global Wildland Fire Emission Model (GWEM): Evaluating the use of global area burnt satellite data, *J. Geophys. Res.*, *109*, D14S04 doi:10.1029/2003JD003666.
- Jaegle, L., R. V. Martin, K. Chance, L. Steinberger, T. P. Kurosu, D. J. Jacob, A. I. Modi, V. Yoboue, L. Sigha-Nkamdjou, and C. Galy-Lacaux (2004), Satellite mapping of rain induced nitric oxide emissions from soils, *J. Geophys. Res.*, *109*, D21310, doi:10.1029/2004JD004787.
- Jaegle, L., L. Steinberger, R. V. Martin, and K. Chance (2005), Global partitioning of NOx sources using satellite observations: Relative roles of fossil fuel combustion, biomass burning and soil emissions, *Faraday Discuss.*, *130*, 407–433, doi:10.1039/b502128f.
- Joshi, V. (1991), Biomass burning in India, in *Global Biomass Burning: Atmospheric, Climatic, and Biospheric Implications*, edited by J. S. Levine, pp. 185–193, MIT Press, Cambridge, Mass.
- Kramer, L. J., R. J. Leigh, J. J. Remedios, and P. S. Monks (2008), Comparison of OMI and ground-based in situ and MAX-DOAS measurements of tropospheric nitrogen dioxide in an urban area, *J. Geophys. Res.*, *113*, D16S39, doi:10.1029/2007JD009168.
- Krijger, J. M., M. van Weele, I. Aben, and R. Frey (2007), Technical Note: The effect of sensor resolution on the number of cloud-free observations from space, *Atmos. Chem. Phys.*, *7*, 2881–2891.
- Kunhikrishnan, T., and M. G. Lawrence (2004), Sensitivity of NO₂ over the Indian Ocean to emissions from the surrounding continents and nonlinearities in atmospheric chemistry responses, *Geophys. Res. Lett.*, *31*, L15109, doi:10.1029/2003GL020210.
- Lamsal, L. N., R. V. Martin, A. van Donkelaar, M. Steinbacher, E. A. Celarier, E. Bucsela, E. J. Dunlea, and J. P. Pinto (2008), Ground-level nitrogen dioxide concentrations inferred from the satellite-borne Ozone Monitoring Instrument, *J. Geophys. Res.*, *113*, D16308, doi:10.1029/2007JD009235.
- Lamsal, L. N., R. V. Martin, A. van Donkelaar, E. A. Celarier, E. J. Bucsela, K. F. Boersma, R. Dirksen, C. Luo, and Y. Wang (2010), Indirect validation of tropospheric nitrogen dioxide retrieved from the OMI satellite instrument: Insight into the seasonal variation of nitrogen oxides at northern mid-latitudes, *J. Geophys. Res.*, *115*, D05302, doi:10.1029/2009JD013351.
- Lamsal, L. N., R. V. Martin, A. Padmanabhan, A. van Donkelaar, Q. Zhang, C. E. Sioris, K. Chance, T. P. Kurosu, and M. J. Newchurch (2011), Application of satellite observations for timely updates to global anthropogenic NOx emission inventories, *Geophys. Res. Lett.*, *38*, L05810, doi:10.1029/2010GL046476.
- Lee, C. J., J. R. Brook, G. J. Evans, R. V. Martin, and C. Mihele (2011), Novel application of satellite and in-situ measurements to map surface-level NO₂ in the Great Lakes region, *Atmos. Chem. Phys.*, *11*, 11761–11775, doi:10.5194/acp-11-11761-2011.
- Leue, C., M. Wenig, T. Wagner, O. Klimm, U. Platt, and B. Jahne (2001), Quantitative analysis of NO₂ emissions from GOME satellite image sequences, *J. Geophys. Res.*, *106*, 5493–5505.
- Luo, M., S. Gluck, M. Madatyán, and D. Shepard (2007), Tropospheric Emission Spectrometer: Level 3 (L3) Dataplot User's Guide, JPL D-41884, v1.0, December 2007.
- Martin, R. V., D. J. Jacob, K. Chance, T. P. Kurosu, P. I. Palmer, and M. J. Evans (2003), Global inventory of nitrogen oxide emissions constrained by space-based observations of NO₂ columns, *J. Geophys. Res.*, *108* (D17), 4537–4548, doi:10.1029/2003JD003453.
- Martin, R. V., C. E. Sioris, K. Chance, T. B. Ryerson, T. H. Bertram, P. J. Woolridge, R. C. Cohen, J. A. Neuman, A. Swanson, and F. M. Flocke (2006), Evaluation of space-based constraints on global nitrogen oxide emissions with regional aircraft measurements over and downwind of eastern North America, *J. Geophys. Res.*, *111*, D15308, doi:10.1029/2005JD006680.
- Martin, R. V., B. Sauvage, I. Folkins, C. E. Sioris, C. Boone, P. Bernath, and J. Ziemke (2007), Space-based constraints on the production of nitric oxide by lightning, *J. Geophys. Res.*, *112*, D09309, doi:10.1029/2006JD007831.
- Müller, J. F., and T. Stavrou (2005), Inversion of CO and NOx emissions using the adjoint of the IMAGES model, *Atmos. Chem. Phys.*, *5*, 1157–1186, doi:10.5194/acp-5-1157-2005.
- Nassar, R., et al. (2008), Validation of Tropospheric Emission Spectrometer (TES) nadir ozone profiles using ozonesonde measurements, *J. Geophys. Res.*, *113*, D15S17, doi:10.1029/2007JD008819.
- Panella, M., V. Tommasini, M. Binotti, L. Palin, and G. Bona (2000), Monitoring nitrogen dioxide and its effects on asthmatic patients: Two different strategies compared, *Environ. Monit. Assess.*, *63*, 447–458.
- Paramee, S., A. Chidthaisong, S. Towprayoon, P. Asnachinda, V. N. Bashkin, and N. Tangtham (2005), Three-year monitoring results of nitrate and ammonium wet deposition in Thailand, *Environ. Monit. Assess.*, *102*, 27–40, doi:10.1007/s10661-005-1593-9.
- Purkait, N. N., S. De, S. Sen, and D. K. Chakrabarty (2009), Surface ozone and its precursors at its two sites in the northeast coast of India, *Indian J. Radio Space Phys.*, *38*, 86–97.
- Reddy, R. R., K. R. Gopal, K. Narasimhulu, L. S. S. Reddy, K. R. Kumar, Y. N. Ahammed, T. V. R. Rao, and P. A. Azeem (2009), Diurnal and seasonal variabilities in surface ozone and its precursor gases at a semi arid site Anantapur (14.62°N, 77.65°E, 331 masl) in India, *Int. J. Environ. Studies*, *65*, 247–226.
- Richter, A., J. P. Burrows, H. Nub, C. Granier, and U. Niemeier (2005), Increase in tropospheric nitrogen dioxide over China observed from space, *Nature*, *437*, 129–132.
- Roy, D. P., J. S. Borak, S. Devadiga, R. E. Wolfe, M. Zheng, and J. Desclotres (2002), The MODIS Land product quality assessment approach, *Remote Sensing Environ.*, *83*, 62–76.
- Sahu, S. K. (2010), Emission inventories of major atmospheric pollutants for India using GIS technique and their impact on the distribution of tropospheric ozone, PhD thesis, Atmospheric and Space Science, University of Pune, Pune, India.
- Samoli, E., et al. (2006), Short term effects of nitrogen dioxide and mortality: An analysis within the APHEA project, *Eur. Respir. J.*, *27*, 1129–1137.
- Seinfeld, J. H., and S. N. Pandis (2006), From air pollution to climate change, in *Atmospheric Chemistry and Physics*, 2nd Ed. John Wiley, New York.
- Sharma, S. K., A. A. Datta, T. T. Saud, M. M. Saxena, T. K. Mandal, Y. N. Ahammed, and B. C. Arya (2010), Seasonal variability of ambient NH₃, NO, NO₂ and SO₂ over Delhi, *J. Environ. Sci. (China)*, *22*, 1023–1028.
- Sharma, S. K., M. Saxena, T. K. Mandal, Y. N. Ahammed, H. Pathak, A. Datta, T. Saud, and B. C. Arya (2011), Variations in mixing ratios of ambient ammonia, nitric oxide and nitrogen dioxide in different environments of India, *Earth Sci. Climate Change*, *1*, <http://dx.doi.org/10.4172/2157-7617.1000102>.
- Smith, B. J., M. Nitschke, L. S. Pilotto, R. E. Ruffin, D. L. Pisaniello, and K. J. Willson (2000), Health effects of daily indoor nitrogen dioxide exposure in people with asthma, *Eur. Respir. J.*, *16*, 879–885.
- Spicer, C. W. (1982), Nitrogen oxide reactions in the urban plume of Boston, *Science*, *215*, 1095–1097.
- van der A, R. J., D. H. M. U. Peters, H. Eskes, K. F. Boersma, M. Van Roozendael, I. De Smedt, and H. M. Kelder (2006), Detection of the trend and seasonal variation in tropospheric NO₂ over China, *J. Geophys. Res.*, *111*, D12317, doi:10.1029/2005JD006594.
- van der A, R. J., H. J. Eskes, K. F. Boersma, T. P. C. Van Noije, M. Van Roozendael, I. De Smedt, D. H. M. U. Peters, and E. W. Meijer (2008), Trend, seasonal variability and dominant NOx sources derived from a ten year record of NO₂ measured from space, *J. Geophys. Res.*, *113*, D04302, doi:10.1029/2007JD009021.
- Venkataraman, C., G. Habib, D. Kadamba, M. Shrivastava, J.-F. Leon, B. Crouzille, O. Boucher, and D. G. Streets (2006), Emissions from open biomass burning in India: Integrating the inventory approach with high-resolution Moderate Resolution Imaging Spectroradiometer (MODIS) active-fire and land cover data, *Global Biogeochem. Cycles*, *20*, GB2013, doi:10.1029/2005GB002547.
- Wiedinmyer, C., et al. (2011), The Fire Inventory from NCAR (FINN): A high resolution global model to estimate the emissions from open burning, *Geosci. Model Dev.*, *4*, 625–641.
- Wenig, M. O., A. M. Cede, E. J. Bucsela, E. A. Celarier, F. K. Boersma, J. P. Veefkind, E. J. Brinksma, J. F. Gleason, and J. R. Herman (2008), Validation of OMI tropospheric NO₂ column densities using direct-sun mode Brewer measurements at NASA Goddard Space Flight Center, *J. Geophys. Res.*, *113*, D16S45, doi:10.1029/2007JD008988.
- Worden, J., S. S. Kulawik, M. Shepard, S. Clough, H. Worden, K. Bowman, and A. Goldman (2004), Predicted errors of tropospheric emission spectrometer nadir retrievals from spectral window selection, *J. Geophys. Res.*, *109*, D09308, doi:10.1029/2004JD004522, 2004.
- Worden, J., D. B. A. Jones, J. Liu, M. Parrington, K. Bowman, I. Stajner, R. Beer, J. Jiang, V. Thouret, S. Kulawik, J. F. Li, S. Verma, and H. Worden (2009), Observed vertical distribution of tropospheric ozone during the Asian summertime monsoon, *J. Geophys. Res.*, *114*, D13304, doi:10.1029/2008JD010560.
- Yienger, J. J. and H. Levy (1995), Empirical model of global soil-biogenic NOx emissions, *J. Geophys. Res.*, *100*, 11447–11464.
- Zhang, Q., et al. (2007), NOx emission trends for China, 1995–2004: The view from the ground and the view from space, *J. Geophys. Res.*, *112*, D22306, doi:10.1029/2007JD008684.
- Zhang, Q., et al. (2009), Asian emissions in 2006 for the NASA INTEX-B mission, *Atmos. Chem. Phys.*, *9*, 5131–5153.